Received: 7 January 2024 | Revised: 22 March 2024 | Accepted: 2 April 2024

DOI: 10.1002/idm2.12170

RESEARCH ARTICLE

Interdisciplinary Materials — Open Access — WILEY

Manipulation of metavalent bonding to stabilize metastable phase: A strategy for enhancing zT in GeSe

Yilun Huang[1] | **Tu Lyu**[1,2] | **Manting Zeng**[1] | **Moran Wang**[1] | **Yuan Yu**[3] | **Chaohua Zhang**[1] | **Fusheng Liu**[1] | **Min Hong**[4] | **Lipeng Hu**[1]

[1]College of Materials Science and Engineering, Guangdong Provincial Key Laboratory of Deep Earth Sciences and Geothermal Energy Exploitation and Utilization, Shenzhen University, Shenzhen, China

[2]College of Physics and Optoelectronic Engineering, Shenzhen University, Shenzhen, China

[3]Institute of Physics (IA), RWTH Aachen University, Aachen, Germany

[4]Center for Future Materials and School of Engineering, University of Southern Queensland, Springfield Central, Queensland, Australia

Correspondence
Tu Lyu and Lipeng Hu, College of Materials Science and Engineering, Guangdong Provincial Key Laboratory of Deep Earth Sciences and Geothermal Energy Exploitation and Utilization, Shenzhen University, Shenzhen 518060, China.
Email: tulyu@szu.edu.cn and hulipeng@szu.edu.cn

Min Hong, Center for Future Materials and School of Engineering, University of Southern Queensland, Springfield Central, Queensland 4300, Australia.
Email: min.hong@usq.edu.au

Funding information
National Key R&D Program of China, Grant/Award Number: 2021YFB1507403; National Natural Science Foundation of China, Grant/Award Number: 52071218; China Postdoctoral Science Foundation, Grant/Award Number: 2022M722170; Shenzhen University 2035 Program for Excellent Research, Grant/Award Number: 00000218

Abstract

Exploration of metastable phases holds profound implications for functional materials. Herein, we engineer the metastable phase to enhance the thermoelectric performance of germanium selenide (GeSe) through tailoring the chemical bonding mechanism. Initially, $AgInTe_2$ alloying fosters a transition from stable orthorhombic to metastable rhombohedral phase in GeSe by substantially promoting *p*-state electron bonding to form metavalent bonding (MVB). Besides, extra Pb is employed to prevent a transition into a stable hexagonal phase at elevated temperatures by moderately enhancing the degree of MVB. The stabilization of the metastable rhombohedral phase generates an optimized bandgap, sharpened valence band edge, and stimulative band convergence compared to stable phases. This leads to decent carrier concentration, improved carrier mobility, and enhanced density-of-state effective mass, culminating in a superior power factor. Moreover, lattice thermal conductivity is suppressed by pronounced lattice anharmonicity, low sound velocity, and strong phonon scattering induced by multiple defects. Consequently, a maximum zT of 1.0 at 773 K is achieved in $(Ge_{0.98}Pb_{0.02}Se)_{0.875}(AgInTe_2)_{0.125}$, resulting in a maximum energy conversion efficiency of 4.90% under the temperature difference of 500 K. This work underscores the significance of regulating MVB to stabilize metastable phases in chalcogenides.

KEYWORDS
band structure, GeSe, metastable phase, metavalent bonding, thermoelectric

Yilun Huang and Tu Lyu contributed equally to this work.

1 | INTRODUCTION

Crystalline solids from the periodic aggregation of atoms result in sophisticated phases, encompassing thermodynamically stable states and kinetically trapped metastable states.[1] Energy is the main difference between these states.[2] Specifically, the stable phase reaches the lowest energy state, while the metastable phase situates at a higher energy state.[3] Despite the relatively higher energy state, it is likely to form the metastable phase under ambient conditions,[4] as evidenced by crystalline carbon in the form of diamond.[5] In materials science and engineering, an in-depth understanding of metastable phases is indispensable given their substantial influences on the microstructure, electronic band structure, and consequently the mechanical/physical/chemical performance of advanced structural and functional materials.[6]

The exploration of metastable phases can potentially advance thermoelectric (TE) energy conversion materials, a cutting-edge technique enabling the direct conversion between heat and electricity.[7–12] The TE devices are potentially used in diverse fields, such as space exploration project[13] and fifth-generation (5G) communication technology.[14] The TE energy conversion efficiency is determined by the materials' dimensionless figure of merit $zT = \alpha^2\sigma T/\kappa$,[15] an attribute that is closely related to phase structures, including stable and metastable phases.[16] Herein α, σ, T, and κ denote the Seebeck coefficient, electrical conductivity, absolute temperature, and the thermal conductivity (including the lattice thermal conductivity κ_L and electronic thermal conductivity κ_e), respectively.[17–22]

Metastable phases in some TE materials are predicted to exhibit higher zT compared with their stable counterparts.[16] For instance, the metastable cubic Cu_2SnSe_3 was reported to yield a higher zT than the stable monoclinic phase due to desirable electronic band structures of the former.[23] However, procuring the metastable phase at ambient temperature presents a significant challenge. As per Ostwald's rule, the solid phase formed during the crystallization process favors the metastable phase rather than the stable phase.[24] Yet, with decreasing the temperature, the metastable phase gradually transforms into the stable phase. Strategies of quenching or rapid cooling and multicomponent alloying can lead to the metastable phase.[25,26] However, even weak driving forces, like thermal cycling, can trigger the transition to a stable state.[4] Such transition undermines the superior TE performance of the metastable phase, thereby obstructing the prolonged functionality of TE devices, particularly in intermediate- and high-temperature TE power generations. Therefore, exploring strategies to stabilize these metastable phases, despite their intrinsically higher free energy compared to the equilibrium states, holds both academic and practical significance for the TE community.

Germanium selenide (GeSe) serves as a particularly insightful system for scrutinizing the impact of metastable phases on TE performance. This primarily arises from its sophisticated crystal structures, encompassing the stable orthorhombic and hexagonal (achieved by substituting 25% Te on Se sites) phases formed under ambient conditions, alongside the metastable rhombohedral and cubic phases that result from the transformation of orthorhombic phase by multicomponent alloying.[27–30] Both theoretical and experimental evidence corroborate that metastable phases of GeSe have excellent TE performance compared to their stable counterparts,[29,31] driven by the unique electronic band structure and phonon dispersion. Nevertheless, the potential transition from metastable to stable phases during thermal cycling could provoke a sudden degradation in TE performance. Hence, innovative strategies are imperative to secure the metastable phase across the entire temperature range, thereby propelling the average zT (zT_{ave}) of GeSe to higher plateaus.

The phase structure is inherently determined by the chemical bonding mechanisms, a trait predominantly governed by atomic orbital interactions.[32] Hence, regulating chemical bonds through manipulating the atomic orbital interactions offers a pathway to stabilize the metastable phases. Recent findings have unveiled a distinct correlation between the disparate crystal structures of GeSe and their respective chemical bonding mechanisms.[28,33,34] Specifically, the stable orthorhombic and hexagonal phases are characterized by covalent bonding, where adjacent atoms share one electron pair.[35] Contrastingly, the metastable rhombohedral and cubic phases utilize a distinctive bonding modality established via a half-filled σ-bond between p-orbital electrons, which involves the sharing of approximately one electron between neighbor atoms.[36,37] This atypical bond is referred to as metavalent bonding (MVB).[38] The alterations in the degree of p–p electrons bonding can trigger a significant shift in the chemical bonding paradigm from covalent bonding to MVB,[33] which presents a viable approach to prepare and stabilize the metavalently bonded rhombohedral or cubic phase, thereby addressing the aforementioned challenges.

In this work, as schematically summarized in Figure 1, we elucidate that alloying orthorhombic GeSe with $AgInTe_2$ tailors the chemical bonding mechanism from conventional covalent bonding to MVB by significantly strengthening p–p orbital electrons interactions, which promotes a metastable rhombohedral phase at ambient temperature. However, an obstacle arises as this

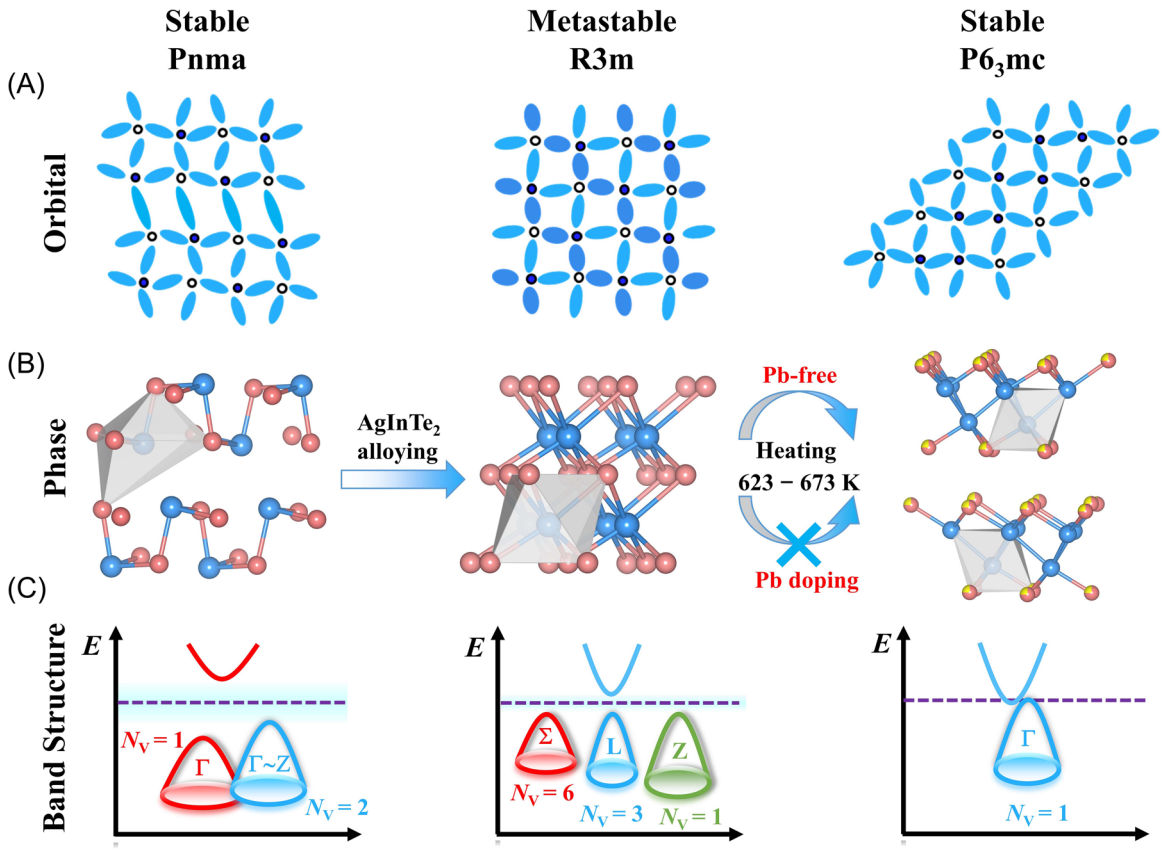

FIGURE 1 Schematic representation of orbital interactions to achieve and stabilize the metastable rhombohedral phase. (A) Different phase structures depend on their orbital interactions and thus the chemical bonding mechanism. (B) The $AgInTe_2$ alloying catalyzes the transition from orthorhombic to rhombohedral phase in germanium selenide (GeSe) by tailoring the chemical bonding mechanism from covalent bonding to metavalent bonding. This metastable rhombohedral phase reverts to the stable hexagonal phase under thermal cycling, but Pb doping secures the rhombohedral phase at elevated temperatures. (C) The metastable rhombohedral phase shows a more suitable bandgap compared to the stable orthorhombic and hexagonal phases. Meanwhile, the convergence of multiple valence bands in the metastable rhombohedral phase indicates a large band degeneracy (N_v). All these characteristics are in favor of a high thermoelectric performance.

thermoelectrically favorable rhombohedral phase reverts to the undesired orthorhombic or hexagonal phases at approximately 630–650 K, occasioning an abrupt deterioration in TE performance. Through electron localization function (ELF) calculations, we reveal that trace amounts of Pb serve to secure the metastable rhombohedral phase against thermal cycling via suppressing the *s*–*p* orbital hybridization and thereupon further intensifying the *p*-state electrons bonding. Consequently, a superior zT of 1.0 at 773 K and a substantially enhanced zT_{ave} of 0.53 between 298 and 773 K are achieved in $(Ge_{0.98}Pb_{0.02}Se)_{0.875}(AgInTe_2)_{0.125}$. Additionally, a pioneering single-leg GeSe-based TE device is fabricated, showcasing a maximum energy conversion efficiency of 4.90% and power density of 1.12 W cm^{-2} under a temperature difference of 500 K. This work not only underscores the significance of stabilizing metastable phases in *p*-bonded chalcogenides through regulating the degree of MVB but also opens avenues for their tailored applications in advanced TE systems.

2 | RESULTS AND DISCUSSION

Figure 2A presents the room temperature powder X-ray diffraction (XRD) patterns of as-synthesized $(Ge_{1-y}Pb_ySe)_{1-x}(AgInTe_2)_x$, compared with the standard patterns of orthorhombic (*Pnma*) and rhombohedral (*R*3*m*) structures. The XRD pattern of pristine GeSe matches well with the standard patterns of the orthorhombic phase (JCPDS #48-1226). As for the XRD patterns of samples alloyed with $AgInTe_2$, there exist extra duplex peaks near 43°–45°, indicating the existence of a rhombohedral phase.[31,39] As the $AgInTe_2$ content increases to ≥0.075, the three characteristic diffraction peaks of the orthorhombic phase between 31° and 33° merge into a single peak, demonstrating that the rhombohedral phase is completely formed in $(GeSe)_{1-x}(AgInTe_2)_x$. Such phase evolution is further examined by transmission electron microscopy (TEM) analyses on the typical sample of $(GeSe)_{0.875}(AgInTe_2)_{0.125}$, as shown in Supporting Information S1: Figure S1. Specifically, TEM images show domain structures and Ge vacancy layers,

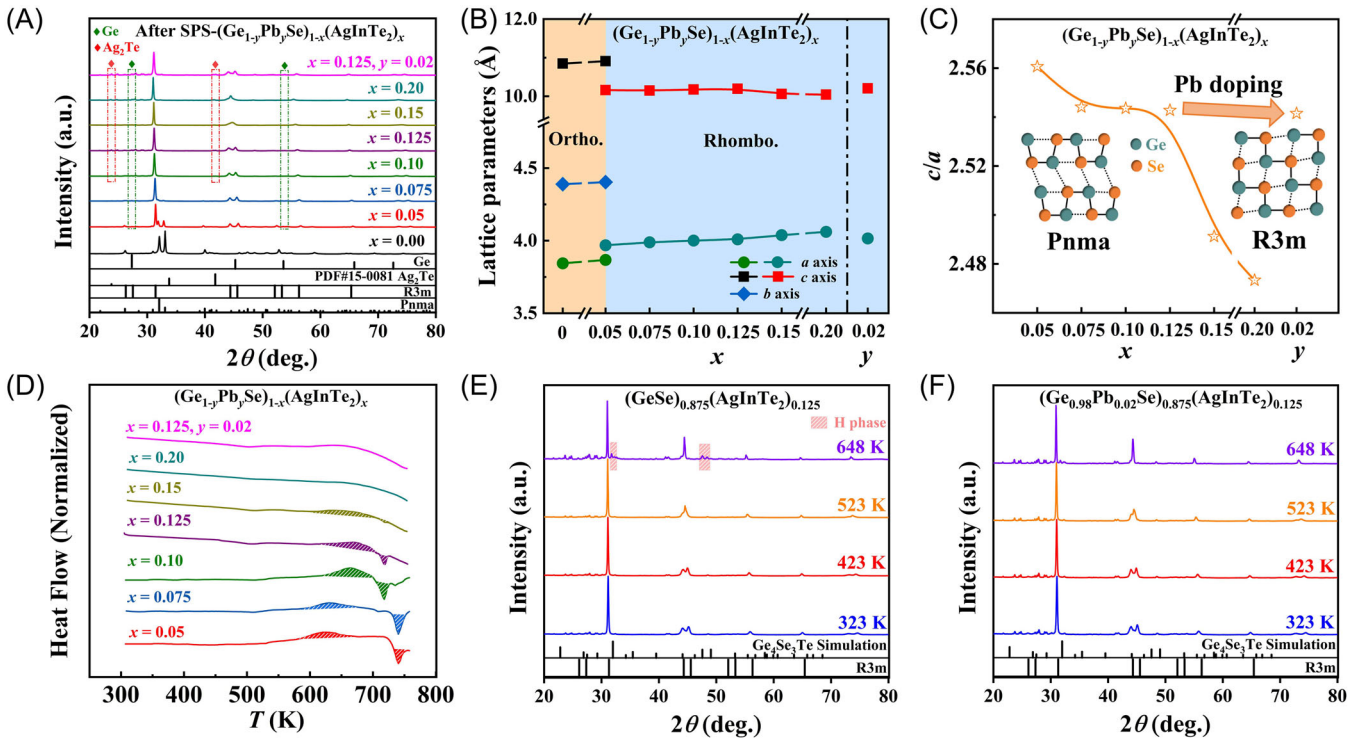

FIGURE 2 Phase evolution with $AgInTe_2$ alloying and Pb doping in germanium selenide (GeSe). (A) Room temperature powder X-ray diffraction (XRD) patterns of $(Ge_{1-y}Pb_ySe)_{1-x}(AgInTe_2)_x$. (B) Lattice parameters and (C) value of c/a calculated by Rietveld refinement. (D) Differential scanning calorimeter (DSC) analyses. In situ XRD patterns of (E) $(GeSe)_{0.875}(AgInTe_2)_{0.125}$ and (F) $(Ge_{0.98}Pb_{0.02}Se)_{0.875}(AgInTe_2)_{0.125}$, confirming that Pb can eliminate the hexagonal phase at elevated temperatures.

which exclusively exist in rhombohedral phase,[40] and the selected area electron diffraction patterns are indexed to the rhombohedral phase. This substantiates that $AgInTe_2$ alloying enhances the crystal symmetry of GeSe and concurrently stimulates the Ge precipitation.[26] This explains the observation of Ge secondary phases in the XRD patterns. Moreover, the impurity peaks corresponding to Ag_2Te are also found in the XRD patterns of $(Ge_{1-y}Pb_ySe)_{1-x}(AgInTe_2)_x$,[41] which is further examined by the backscattered imaging mode of scanning electron microscopy and energy dispersive X-ray spectroscopy analyses (Supporting Information S1: Figures S3–S5).

The phase transition interplay between stable orthorhombic and metastable rhombohedral phases is fundamentally contingent on the alterations of the chemical bonding mechanisms.[37] Specifically, the stable orthorhombic GeSe utilizes covalent bonding, leveraging *p–p* orbital electron interactions with *s–p* orbital hybridization.[42] The orthorhombic phase is characterized by the lower effective coordination numbers (CN = 3), corresponding to an equivalent count of covalent bonds. In contrast, the metastable rhombohedral phase demonstrates the presence of MVB, with a total count of 6 valence electrons and a corresponding CN of 6, as signified by 6 half-filled σ-bonds among *p*-orbital electrons.[37] Such a configuration indicates an inappreciable *s–p* orbital hybridization and an amplification of *p–p* electrons bonding, thereby aligning the σ-bond within the rhombohedral phase.

The formation of MVB and thereby the σ-bond alignment is characterized by a diminished ratio of long to short bond length, favoring reduced Peierls distortions.[38] This subsequently enhances the crystal symmetry from orthorhombic to rhombohedral phase in GeSe as reflected in the altered lattice parameters. Figure 2B demonstrates the lattice parameters of $(Ge_{1-y}Pb_ySe)_{1-x}(AgInTe_2)_x$ calculated by Rietveld refinement using the XRD patterns. The pristine GeSe displays the different *a, b*, and *c* axis, attributable to the strong Peierls distortions in the orthorhombic phase.[43] In contrast, $AgInTe_2$ alloying gradually enlarges the a (=b) axis while contracting the *c* axis in the metastable rhombohedral phase. Furthermore, the calculated c/a value declines from approximately 2.543 for $x = 0.075$–0.125 samples to around 2.473 as the $AgInTe_2$ content ascends to $x = 0.20$ (Figure 2C). This implies that $AgInTe_2$ alloying effectively transforms the chemical bonding mechanism to MVB and promotes the alignment of σ-bond.

The metastable phase tends to revert to a more thermodynamically stable state under thermal driving

forces.[4] The differential scanning calorimeter (DSC) analysis was conducted to scrutinize the stability of this metastable phase across the entire temperature range. As depicted in Figure 2D, the conspicuous exothermic peaks ($x = 0.05$–0.15) signify the instability of the metastable rhombohedral phase as the temperature rises.[27] Intriguingly, the phase transition mechanism exhibits discrepancies depending on the variation of the x value. For instance, an exothermic peak appearing at approximately 630 K in samples with $x = 0.05$ and 0.075 points to a transition from metastable rhombohedral to stable orthorhombic phase. Differently, an exothermic peak at roughly 650 K in samples with $x = 0.10$–0.15 is consistent with a transition from metastable rhombohedral to a stable hexagonal phase. This phenomenon can be interpreted by the phase diagram of $GeSe_{1-m}Te_m$, where the hexagonal phase materializes when m ranges from 0.15 to 0.35.[44] Meanwhile, the endothermic peak at elevated temperatures marks a transition from orthorhombic ($x = 0.05$–0.075) or hexagonal ($x = 0.10$–0.15) phase to a cubic one.

Further insights into these phase transitions were gleaned on two typical samples ($x = 0.125$ and $y = 0.02$) through in situ XRD measurements, as shown in Figure 2E,F. According to the XRD patterns, the $x = 0.125$ sample corresponds to the rhombohedral phase from 323 K to 523 K, which is reflected in the single diffraction peak at 31° and the duplex peaks between 43° and 45°. However, the hexagonal phase features appear as the temperature increases to 648 K, as evidenced by the diffraction peaks at around 32° and between 48° and 50° (marked in shadows in Figure 2E). These observations collectively indicate a thermally induced transition from a metastable rhombohedral phase to a stable hexagonal one. The emergence of the hexagonal phase dramatically decreases the TE performance at elevated temperatures,[44] which will be discussed in detail later. Although increasing $AgInTe_2$ content helps retain the metastable rhombohedral phase across the entire temperature range (Figure 2D), the resultant dense point defects could detrimentally impact carrier mobility (μ).[26] Consequently, exploring strategies to further stabilize the metastable rhombohedral phase is of paramount importance.

The stabilization of metastable rhombohedral GeSe fundamentally hinges on further increasing the degree of MVB by mitigating *s*-*p* hybridization and amplifying *p*-state electrons bonding.[33] The extant literature has illustrated that PbTe, characterized by a large energy gap of ~2 eV between the upper valence *s* bands and *p* bands, exhibits challenges for *s*–*p* hybridization, thereby favoring the interactions of *p*-state electrons.[45] Characterized as an MVB compound with a cubic structure, the unique attributes of PbTe suggest that introducing trace amounts of Pb into the $x = 0.125$ sample could stabilize the metastable phase throughout the whole temperature range. This proposition is corroborated by the eliminated exothermic peaks at roughly 650 K from the DSC analysis (Figure 2D) and the disappeared diffraction peaks of the hexagonal phase at 648 K from in situ XRD measurements (Figure 2F). In addition, the refinement of the c/a value further descends to ~2.541 upon 2 at% Pb doping (visible in the inset of Figure 2C), thus verifying the enhanced degree of MVB. This evidence suggests that trace amounts of Pb effectively preclude the adverse phase transition, preserving the metastable state across the entire temperature range.

From a crystallographic perspective, the formation of rhombohedral phase can be elucidated by tracking the migration of Ge atoms toward the second nearest Se atoms. As depicted in Figure 3A, the orthorhombic GeSe comprises threefold Ge/Se units that share vertices, culminating in a chair-like polygon configuration. The three bonds (comprising one vertical and two horizontal short bonds) exhibit relatively equivalent bond lengths of 2.59 Å and bond angles of 93°, a finding congruent with the previous report.[42] These metrics indicate their *p*-type bonding character, albeit with minor *s* orbital hybridization.[42]

By contrast, alloying with $AgInTe_2$ leads to an intriguing alteration of the bonding mechanism, specifically compressing the long bonds and stretching the horizontal short bonds. This rearrangement facilitates the interaction between the central Ge and the second nearest Se, engendering a highly symmetric rhombohedral phase (as illustrated in Figure 3B). However, the count of valence electrons fails to correspond with the total number of bonds as per the classical covalent bonding theory, where each covalent bond is constituted by a pair of electrons.[35] This discrepancy leaves only six valence electrons to populate the 6 available bonds within the octahedral framework.[46] Such an observation postulates that the most plausible way to form these uniquely half-filled σ-bonds is through the MVB, enabled by promoting the bonding of *p*-orbital electrons and suppressing *s*–*p* hybridization.[47]

This proposition is supported by ELF analyses via density functional theory (DFT) calculations. While electrons in covalent bonding exhibit a higher degree of localization, MVB is characterized by more delocalized electrons.[43] As depicted in Figure 3D, the ELF analysis of orthorhombic $Ge_{27}Se_{27}$ reveals the overlap of vertical and horizontal short bonds with a comparatively high ELF value, suggestive of electron localization. Nevertheless, the ELF value in the middle of the long bonds plunges below 0.2, underlining the failure to form

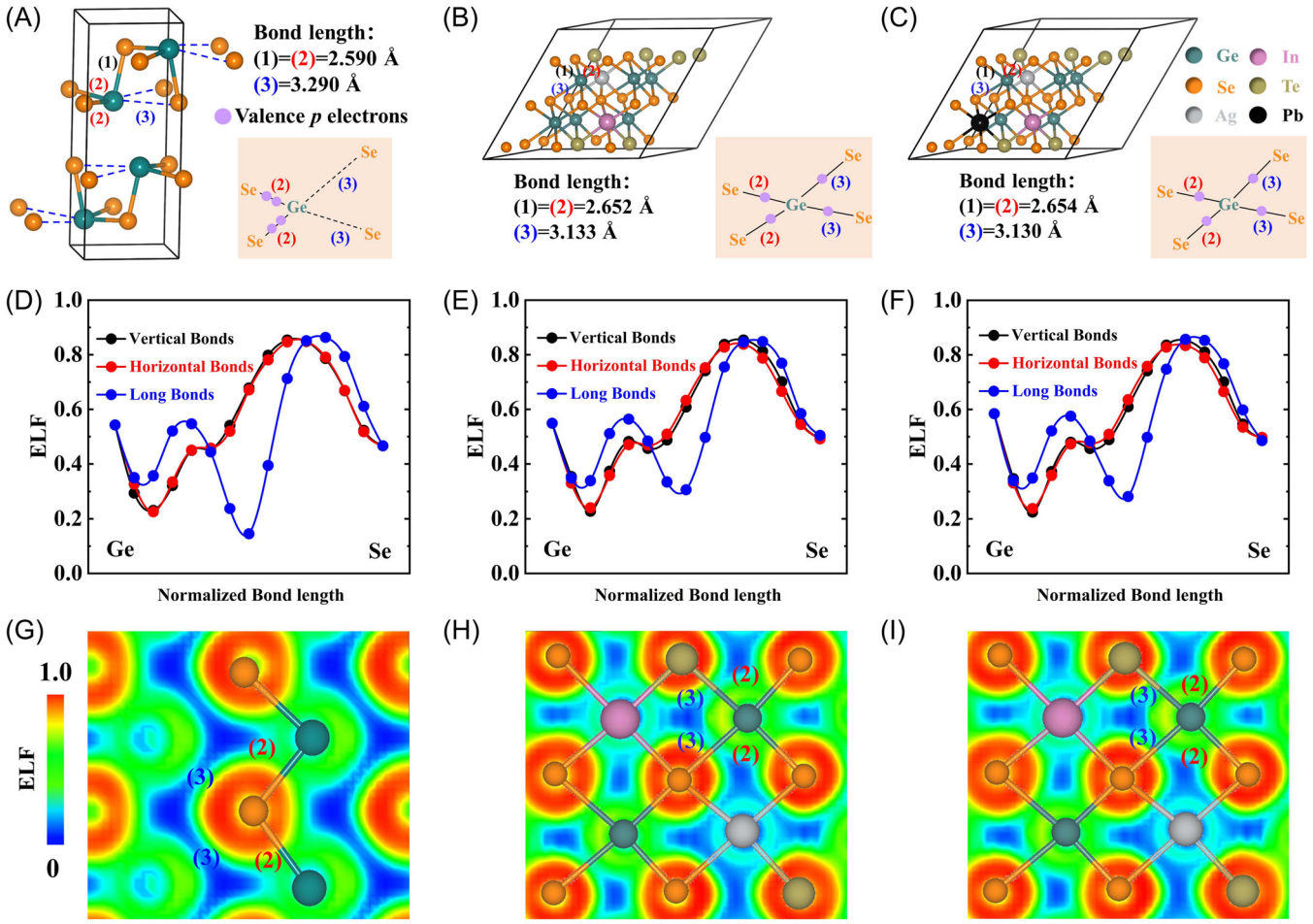

FIGURE 3 Crystal structures of (A) orthorhombic GeSe, (B) rhombohedral GeSe alloying with $AgInTe_2$, and (C) rhombohedral GeSe alloying with $AgInTe_2$ and Pb. Electron localization functions (ELF) of (D) orthorhombic $Ge_{27}Se_{27}$, (E) rhombohedral $Ge_{21}Ag_3In_3Se_{21}Te_6$, and (F) $Ge_{20}PbAg_3In_3Se_{21}Te_6$, as well as their plane profiles (G–I).

covalent bonds as the long Ge-Se pairs are separated by a "vacuum" space, which is scarcely populated by valence electrons. This vacuum area is also discernible in the ELF contour map (Figure 3G), where the blue regions signify a low density of localized electrons. The hexagonal $Ge_{32}Se_{24}Te_8$ embraces the high ELF value for Ge-Se/Te bonds similar to the orthorhombic phase, conforming to its feature of covalent bonding (Supporting Information S1: Figure S8). However, the Ge-Ge bond exists in the hexagonal phase, which differentiates it from the orthorhombic phase (Supporting Information S1: Figures S7 and S8).[48] In the rhombohedral $Ge_{21}Ag_3In_3Se_{21}Te_6$ and $Ge_{20}PbAg_3In_3Se_{21}Te_6$, an increased ELF value in the middle of the long bond (Figure 3E,F) alongside their distinct ELF profile (Figure 3H,I) suggests the amplified interactions between Ge-Se atom pairs in comparison to the orthorhombic counterpart. Furthermore, the addition of Pb mitigates the length difference between the long and short bonds (Figure 3C). This observation corroborates that Pb doping reinforces the degree of MVB and thereby the alignment of σ-bond, solidifying our initial proposition.

Electronic transport properties of TE materials strongly depend upon band structures.[49] To investigate the impact of metastable phase on band structures, we conducted DFT calculations. As plotted in Figure 4A–C, the computed Fermi surface discloses that the band degeneracy (N_v) of the metastable rhombohedral phase is larger than that of the stable orthorhombic or hexagonal phases. Specifically, in orthorhombic GeSe, the N_v equals 3 while both the first valence band (VB_1, $N_v = 2$) along the Γ-Z direction and the second valence band (VB_2, $N_v = 1$) at Γ point actively participate in electrical transport. Unfortunately, it is a formidable task to involve VB_2 in electrical transport due to the ultralow carrier concentration (n).[50] Consequently, the effective N_v of orthorhombic GeSe remains limited to 2. Furthermore, the hexagonal Ge_4Se_3Te embraces the smallest N_v of 1, leading

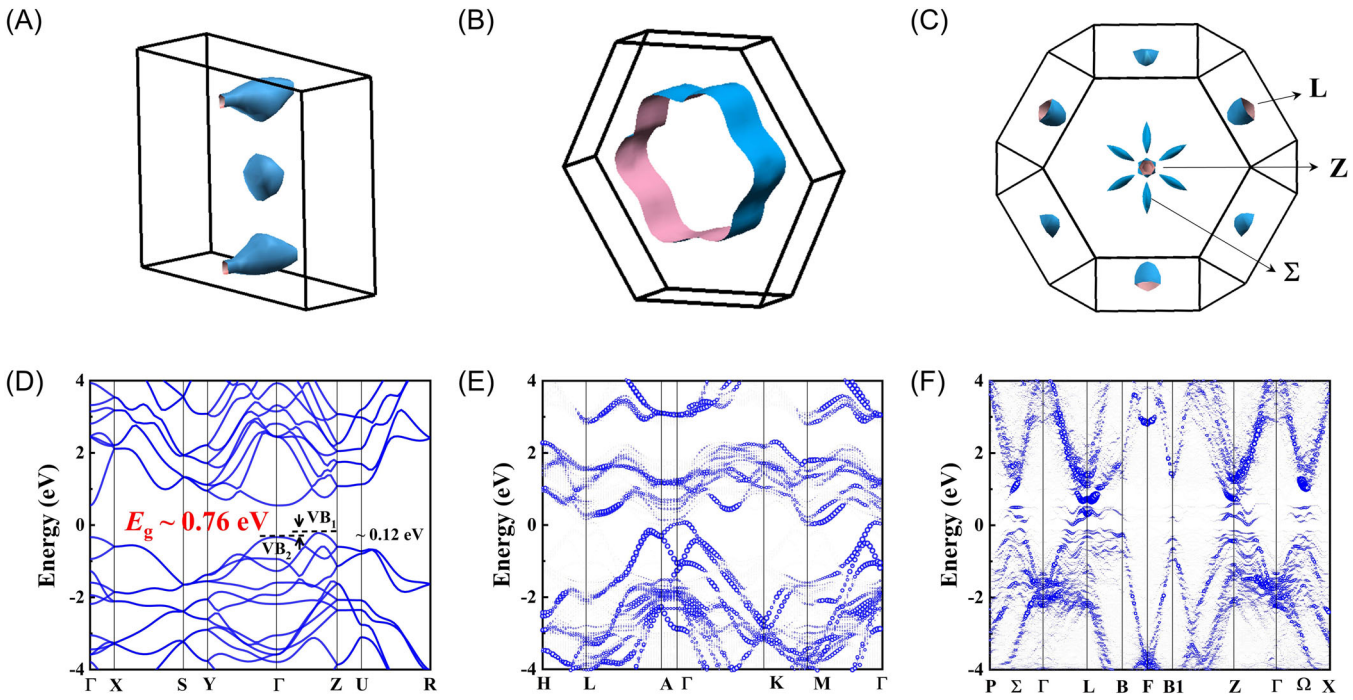

FIGURE 4 Calculated electronic band structures of different phase structures. Fermi surfaces of (A) orthorhombic $Ge_{27}Se_{27}$, (B) hexagonal $Ge_{32}Se_{24}Te_8$, and (C) rhombohedral $Ge_{27}Se_{27}$. Band structures of (D) orthorhombic $Ge_{27}Se_{27}$, (E) hexagonal $Ge_{32}Se_{24}Te_8$, and (F) rhombohedral $Ge_{21}Ag_3In_3Se_{21}Te_6$.

to the lowest density-of-state effective mass (m^*). In stark contrast, in the metastable rhombohedral GeSe, the VB_1 at the L point (L band) exhibits an N_v of 3, the VB_2 at the Σ point (Σ band) possesses an N_v of 6, and an additional valence band (VB_3) near the Z point (Z band) carries an N_v of 1. Such a large N_v in rhombohedral GeSe ensures a higher TE performance compared with the orthorhombic and hexagonal counterparts. In addition, the binary rhombohedral GeSe exhibits an appropriate bandgap (E_g) of 0.45 eV (Supporting Information S1: Figure S9). This value situates between the orthorhombic (E_g = ~0.76 eV, Figure 4D) and hexagonal (absence of E_g, Figure 4E) phases, signifying a respectable electric power factor ($PF = \sigma\alpha^2$) within the rhombohedral phase. However, although there are beneficial band structures in the binary rhombohedral phase, the existence of energy gaps (ΔE) between L and Z occasions constraints on the achievement of ideal electrical properties. Such ΔE could act as barriers, impeding the contributions from the Z band and subsequently diminishing the anticipated positive attributes of the material's band structure.[51] Therefore, resolving these ΔE issues becomes paramount in realizing the full potential of the rhombohedral GeSe.

Regarding this issue, it is discovered that alloying with $AgInTe_2$ promotes more valence bands (L, Σ, and Z bands) to engage in electrical transport. Specifically, these ΔE values are substantially diminished to nearly 0 eV in $Ge_{21}Ag_3In_3Se_{21}Te_6$. The resultant band convergence culminates in a sizable N_v of 10 in the rhombohedral phase (Figure 4C), thereby significantly raising m^* and thus α. This unprecedented discovery of three converging valence bands in rhombohedral GeSe is reported for the first time (Figure 4F). Additionally, although $AgInTe_2$ alloying reduces the E_g of rhombohedral GeSe to 0.13 eV, subsequent Pb doping expands it to 0.22 eV (Supporting Information S1: Figure S10), helping to mitigate the undesirable bipolar effect.[52] It is worth noting that DFT calculations often underestimate the E_g[53]; so, the real E_g may better meet the needs for medium temperature power generation.

The electrical properties of GeSe are markedly influenced by its phase structure, exhibiting conspicuous divergences between stable and metastable phases. As shown in Figure 5A, the stable orthorhombic GeSe exhibits an ultralow carrier concentration (n) of $1.2 \times 10^{16}\,cm^{-3}$ at room temperature stemming from the large E_g and Ge vacancy formation energy (E_v).[26] With the addition of $AgInTe_2$, the n dramatically rises to $2.3 \times 10^{20}\,cm^{-3}$ for the $x = 0.125$ sample that utilizes the metastable rhombohedral phase. The pronounced rise in n is accredited to the alteration of the chemical bonding mechanism. Specifically, the metavalently bonded rhombohedral phase results in a narrower E_g and lower E_v than the covalently bonded orthorhombic phase.[26]

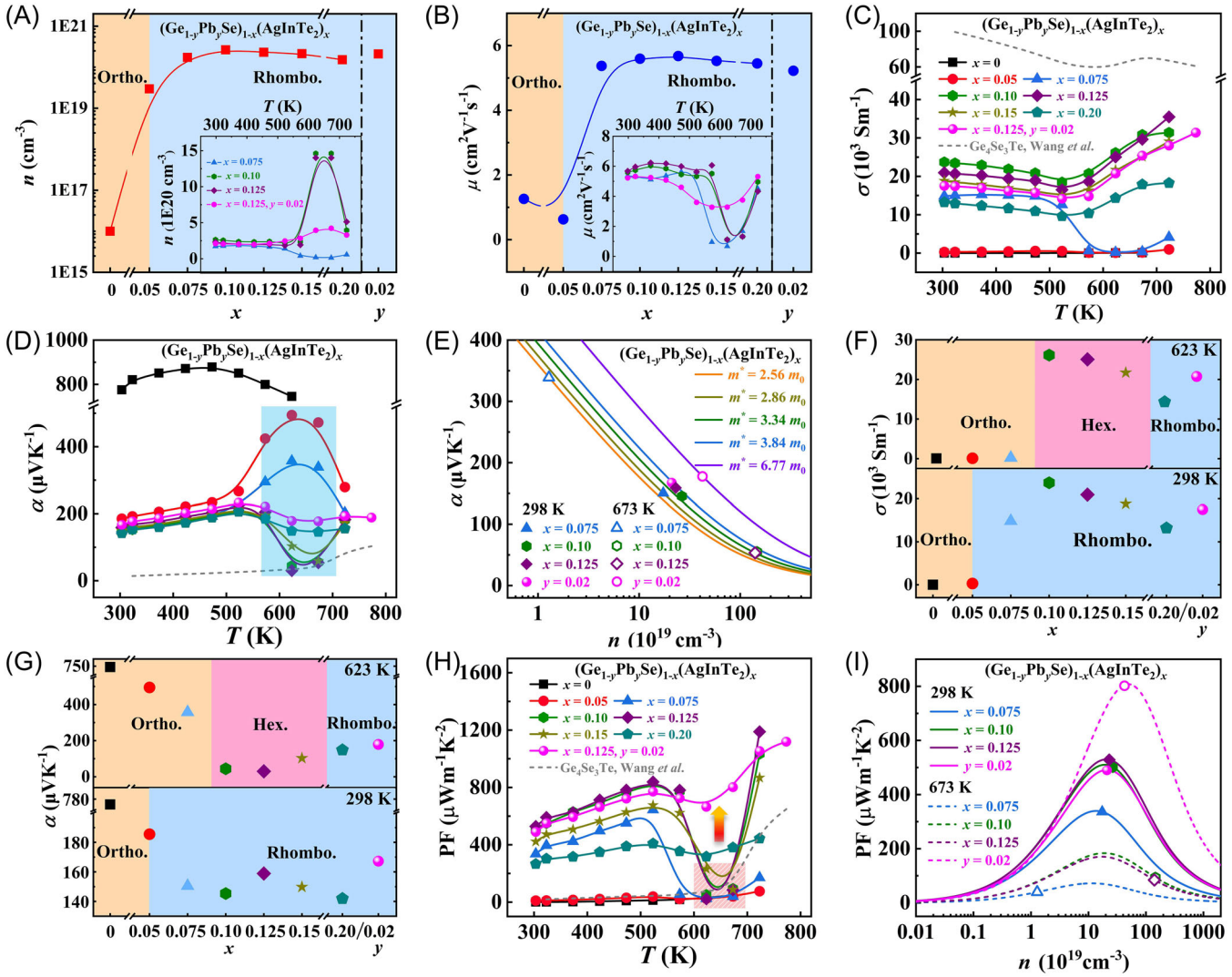

FIGURE 5 Electrical transport parameters of $(Ge_{1-y}Pb_ySe)_{1-x}(AgInTe_2)_x$. (A) Carrier concentration (n) and (B) carrier mobility (μ), as well as the high temperature data of typical samples (insets). Temperature dependence of (C) electrical conductivity (σ) and (D) Seebeck coefficient (α) and the comparison with hexagonal Ge_4Se_3Te.[44] (E) Pisarenko curves calculated by single parabolic band (SPB) model. (F) σ and (G) α of typical samples at different characteristic temperatures. (H) Power factor (PF) as a function of temperature. (I) PF versus n curves calculated by SPB model.

However, the transition from metastable to stable phase has a disastrous effect on n at elevated temperatures (inset of Figure 5A). In particular, the substantial reduction in n at 573 K for the $x = 0.075$ sample is caused by the phase transition to orthorhombic structure, which is characterized by large E_g and E_v.[26] Conversely, the transition to hexagonal phase leads to a surging n for samples with $x = 0.10$ and 0.125, a phenomenon originating from the absence of E_g and subsequent manifestation of metallic behavior. Surprisingly, the n of the Pb-doped sample increases only slightly with the rising temperature, without exhibiting the sharp decline of the typical orthorhombic phase or the spike associated with the hexagonal structure at high temperatures. This behavior is attributed to the fact that Pb doping further enhances the degree of MVB, thus securing the metastable phase against thermal cycling.

Figure 5B demonstrates an ultralow room temperature carrier mobility (μ) of 1.26 $cm^2 V^{-1} s^{-1}$ in stable orthorhombic GeSe, which gradually rises to 5.68 $cm^2 V^{-1} s^{-1}$ as the $AgInTe_2$ content increases to $x = 0.125$. The enhanced μ predominantly stems from the sharper valence band edge of rhombohedral GeSe, leading to a lighter m_b* than its orthorhombic counterpart. This finding is corroborated by DFT calculations (Figure 4 and Supporting Information S1: Figure S9). Conversely, further increasing $AgInTe_2$ content or introducing Pb slightly inhibits μ due to the carrier scattering caused by

point defects. Unfortunately, the transition from metastable to stable phase at elevated temperatures incurs a sudden reduction in μ (inset of Figure 5B), especially for $x = 0.075$ sample that typifies the intrinsically low μ of the orthorhombic phase.[25] A dramatic decrease in μ for $x = 0.10$ and 0.125 samples can be associated with the high n in the hexagonal phase. Remarkably, trace amounts of Pb doping effectively improve the high temperature μ by precluding the transition from metastable to stable phase.

As illustrated in Figure 5C, alloying GeSe with $AgInTe_2$ induces a transition from an orthorhombic to rhombohedral phase, contributing to a significant enhancement in σ by several orders of magnitude owing to the concurrent optimization of n and μ, especially near room temperature. However, for the $x = 0.075$ sample, thermal cycling attracts a transition from the metastable rhombohedral to stable orthorhombic phase at high temperatures, leading to a drastic decline in σ. Conversely, the reversion to the hexagonal phase at high temperatures for $x = 0.10$ and $x = 0.125$ samples sustains the high σ, which is attributed to a surge in n despite the sharply reduced μ. Interestingly, after trace amounts of Pb doping, which stabilizes the rhombohedral phase at elevated temperatures, the σ is slightly lower than the hexagonal one due to the balance of n and μ (Figure 5C). Taking the σ at 673 K as an example, the σ increases from 103 S m^{-1} to 2.9×10^4 S m^{-1} between the stable orthorhombic GeSe and hexagonal $(GeSe)_{0.875}(AgInTe_2)_{0.125}$; then, it slightly drops to 2.5×10^4 S m^{-1} in the metastable rhombohedral $(Ge_{0.98}Pb_{0.02}Se)_{0.875}(AgInTe_2)_{0.125}$.

The α in pristine orthorhombic GeSe reaches an extraordinarily high level and subsequently rapidly diminishes with increasing $AgInTe_2$ content (Figure 5D). This trend is caused by the increased n in the rhombohedral phase. Specifically, the room temperature α declines from 775 to 159 $\mu V K^{-1}$ between the pristine GeSe and $(GeSe)_{0.875}(AgInTe_2)_{0.125}$. Moreover, an abnormal temperature-dependent α is observed at 623–673 K. For instance, temperature-dependent α of the samples with $x = 0.05$ and 0.075 form a peak. Conversely, temperature-dependent α of the samples with $x = 0.10$–0.15 show a valley. The different variation trend is caused by phase transition mechanisms from metastable to stable states at elevated temperature. The former contains the rhombohedral-orthorhombic phase transition, while the latter involves the rhombohedral-hexagonal phase transition, as demonstrated by DSC and in situ XRD analyses. The drastically reduced α in the hexagonal phase region principally originates from its extremely high n, which occasions a significantly reduced PF compared to the rhombohedral counterpart. The strategic addition of Pb effectively intensifies the p–p orbital electrons bonding, thereby promoting the stabilization of the metavalently bonded rhombohedral phase, as substantiated by DFT calculations (Figure 3). This elimination of undesirable phase transition contributes to a relatively excellent α throughout the whole temperature range (Figure 5D). For example, a sharply reduced α of 30 $\mu V K^{-1}$ at 623 K in the $x = 0.125$ sample is significantly amplified to 179 $\mu V K^{-1}$ after 2 at% Pb doping, exhibiting a sixfold increment.

In addition to n, the α is closely relevant to m^*.[54] Figure 5E and Supporting Information S1: Figure S14 depict the Pisarenko lines calculated based on the single parabolic band (SPB) model.[55] Pristine orthorhombic GeSe yields a low m^* value of 0.71 m_0 (Supporting Information S1: Figure S14). By contrast, $AgInTe_2$ alloying tailors the chemical bonding mechanism to MVB, inducing a metastable rhombohedral phase characterized by a half-filled σ-bond. The resulting crystal structure with octahedral coordination exhibits higher symmetry than its orthorhombic counterpart,[47] indicating a large N_v. Moreover, $AgInTe_2$ alloying promotes the convergence of three valence bands (L, Σ and Z bands). Therefore, a high $N_v = 10$ and thus a large $m^* = 3.77$ m_0 are achieved in the $x = 0.125$ sample, surpassing previously reported rhombohedral GeSe ($m^* = 1.8$~3.5 m_0).[26,27,31,56,57] Additionally, we calculated the Pisarenko relationships at 673 K to examine the variation of m^*. The result demonstrates that a reduced m^* of 3.34 m_0 at 673 K is achieved in the $x = 0.125$ sample, which is caused by the transition to a stable hexagonal phase with a small N_v. Contrastingly, 2 at% Pb doping stabilizes the metastable phase by further strengthening the degree of MVB, resulting in a significant increase in m^* from 3.84 m_0 at 298 K to 6.77 m_0 at 673 K. Lastly, we summarize the σ and α as a function of $AgInTe_2$ content x and include a sample with 2 at% Pb doping at different characteristic temperatures (Figure 5F,G). These findings provide a comprehensive understanding of the interplay among the compositions, crystal structures, and performance, accentuating the superior electrical properties of the metastable rhombohedral phase as compared to the stable orthorhombic or hexagonal phases. Such insights underscore the significance of stabilizing metastable phases across the entire temperature range.

The formation of the metavalently bonded metastable rhombohedral phase upon $AgInTe_2$ alloying synergistically optimizes the n, μ, and m^*, leading to a remarkable improvement of PF (Figure 5H). Unfortunately, a sharp decline in PF occurs around 623–673 K, which is predominantly attributed to the transition reverting to the stable orthorhombic or hexagonal phases.

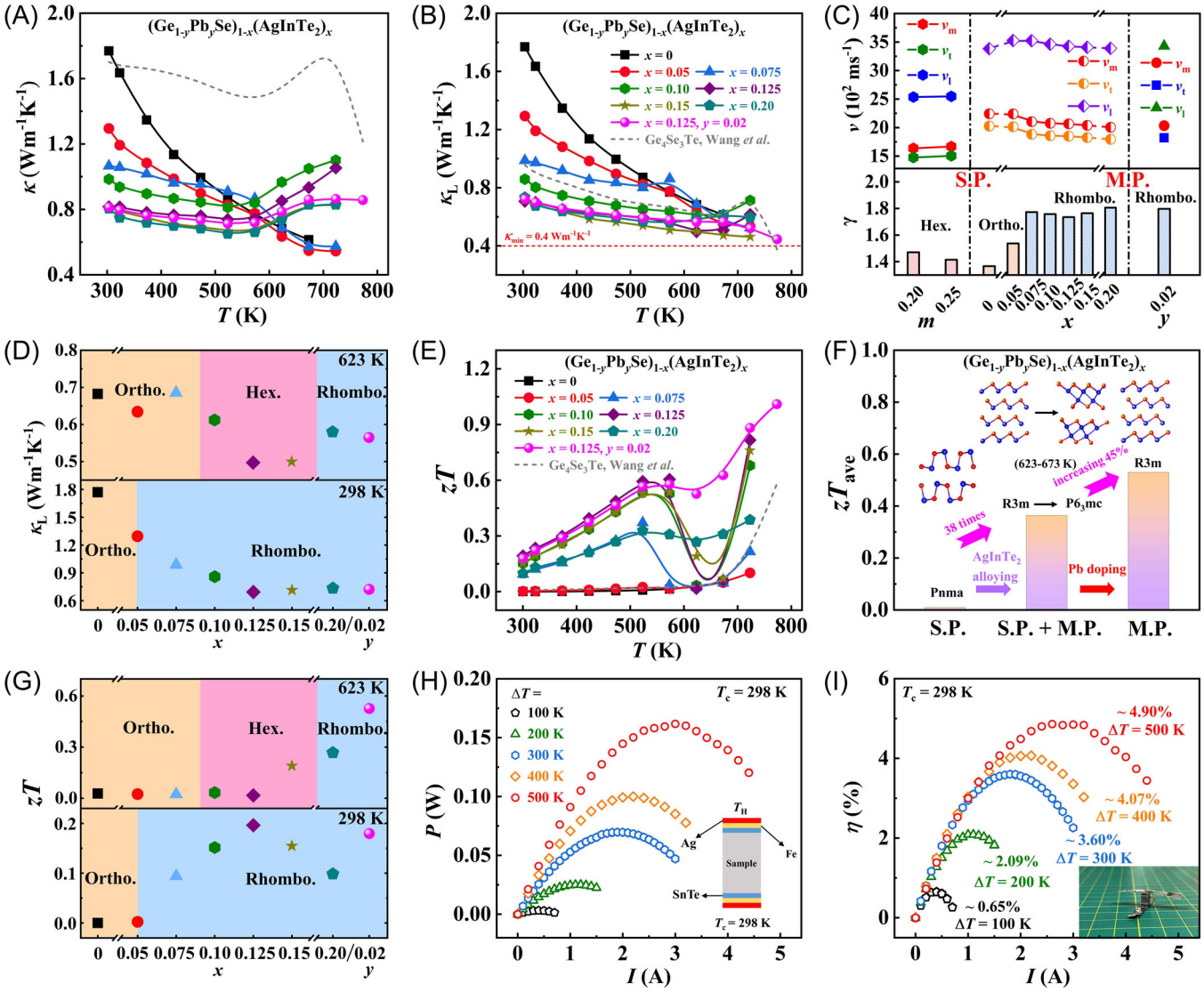

FIGURE 6 Temperature dependence of (A) thermal conductivity (κ) and (B) lattice thermal conductivity (κ_L) of $(Ge_{1-y}Pb_ySe)_{1-x}(AgInTe_2)_x$, compared with hexagonal Ge_4Se_3Te.[44] (C) Top panel: sound velocity (v) and low panel: Grüneisen constants (γ). (D) A plot of κ_L of representative samples at different characteristic temperatures. (E) The figure of merit (zT) as a function of temperature and the contrast with hexagonal Ge_4Se_3Te.[44] (F) The comparison of average zT values among the samples with stable orthorhombic phase (S.P.), the metastable rhombohedral phase that transitions to stable hexagonal phase at elevated temperatures (S.P. + M.P.) and the metastable rhombohedral phase within the entire temperature range (M.P.). (G) zT values of representative samples at different characteristic temperatures. (H) Output power (P) and (I) energy conversion efficiency (η) of the single-leg thermoelectric device under various temperature differences (ΔT).

Surprisingly, even minor Pb doping effectively restrains this adverse phase transition at high temperatures by further strengthening the degree of MVB. Therefore, a substantially enhanced PF of 665 $\mu W\,m^{-1}\,K^{-2}$ at 623 K is secured in the $(Ge_{0.98}Pb_{0.02}Se)_{0.875}(AgInTe_2)_{0.125}$ sample. This value is 30 times greater than the $x = 0.125$ sample that reverts to the hexagonal phase with a PF of 22 $\mu W\,m^{-1}\,K^{-2}$ at 623 K. Furthermore, the relationship between PF versus n, calculated based on the SPB model, underscores the crucial role of stabilizing metastable phase in the PF enhancement (Figure 5I).

The formation and stabilization of the metastable phase through promoting the formation of MVB has a noticeable effect on the thermal properties. As shown in Figure 6A, compared to the stable orthorhombic GeSe, the κ of metastable rhombohedral $(Ge_{1-y}Pb_ySe)_{1-x}(AgInTe_2)_x$ is substantially reduced near room temperature and intermediate temperatures, which mainly derives from the contribution of lattice thermal conductivity (κ_L). By contrast, the enhanced κ at elevated temperatures results from the increased electronic thermal conductivity (κ_e), attributable to the improved σ.

Figure 6B highlights a notable suppression of κ_L in the metastable rhombohedral phase instigated by $AgInTe_2$ alloying and Pb doping. The reduction in κ_L can be elucidated through three aspects. First, the lattice instability of the metavalently bonded rhombohedral phase leads to strong lattice anharmonicity,[58] as mirrored in the increased Grüneisen constant (γ) from 1.3 to 1.5 for the stable orthorhombic (hexagonal) phase to around 1.8 for the metastable rhombohedral counterparts (Figure 6C).[59] Second, the metastable rhombohedral phase features weaker chemical bonding, as only half of an electron pair (one electron) holds the atoms together,[37] which softens the transverse optical modes and diminishes the mean sound velocity (v_m) from 2242 m s^{-1} for stable orthorhombic phase to 2034 m s^{-1} for metastable rhombohedral phase (Figure 6C).[60] Although the hexagonal phase embraces a small v_m (1500–1700 m s^{-1}) and consequently low κ_L, its inferior electrical properties enable a poor zT compared to metastable GeSe. Last, the multiscale lattice defects in the metastable phase, including point defects, domains, and nanoprecipitations, strengthen phonon scattering[61] (Supporting Information S1: Figures S1 and S2). Consequently, a minimum κ_L of ~0.45 W m^{-1} K^{-1} at 773 K is achieved in $(Ge_{0.98}Pb_{0.02}Se)_{0.875}(AgInTe_2)_{0.125}$. A plot of κ_L for representative $(Ge_{1-y}Pb_ySe)_{1-x}(AgInTe_2)_x$ samples at varying characteristic temperatures provides an intuitive indication of the significantly reduced κ_L in the metastable phase (Figure 6D).

The synergistic optimization of electrical and thermal transport properties leads to a significant improvement in the zT. As shown in Figure 6E, a peak zT of 0.82 at 723 K is achieved in the metastable rhombohedral $(GeSe)_{0.875}(AgInTe_2)_{0.125}$, much higher than that of 0.05 at 673 K in the stable orthorhombic GeSe. Unfavorably, the zT_{ave} of 0.37 is not high enough over the entire studied temperature. This is because zT of $(GeSe)_{0.875}(AgInTe_2)_{0.125}$ drops to 0.06 between 623 and 673 K caused by the transition from metastable rhombohedral to stable hexagonal phase at high temperatures. To further increase zT_{ave}, trace amounts of Pb are employed to maintain the metastable phase at high temperatures by further strengthening the degree of MVB. Consequently, a maximum zT of 1.0 at 773 K along with an improved zT_{ave} of 0.53 between 298 and 773 K are achieved in $(Ge_{0.98}Pb_{0.02}Se)_{0.875}(AgInTe_2)_{0.125}$. Such a high zT_{ave} exhibits a 45% enhancement as compared to $(GeSe)_{0.875}(AgInTe_2)_{0.125}$ (Figure 6F). These findings unequivocally affirm that the metastable phase of GeSe offers superior TE performance in comparison to its stable counterpart (Figure 6G).

Using $(Ge_{0.98}Pb_{0.02}Se)_{0.875}(AgInTe_2)_{0.125}$ sample, a single-leg TE device was constructed. The open-circuit voltage (U) rises from 0.02 V to 0.11 V when the temperature difference (ΔT) ranges from 100 K to 500 K (Supporting Information S1: Figure S18). Figure 6H presents the ΔT-dependent output power (P), which exhibits a maximum value of 0.16 W, corresponding to a peak power density of 1.12 W cm^{-2} under a ΔT of 500 K. This value is comparable to that of GeTe-based TE devices.[62] Figure 6I is the current-dependent energy conversion efficiency (η) under disparate ΔT, showing a maximum η of 4.90% under a ΔT of 500 K. This is the first report of a GeSe-based TE device, providing a promising TE candidate for broad applications due to the relatively low materials cost with earth-abundant Se. Furthermore, this work highlights the critical importance of probing the metastable phase in p-bonded chalcogenides and potentially in other TE materials, offering novel insights and opportunities for advancement in the TE field.

3 | CONCLUSIONS

This study develops an innovative approach for preparing and stabilizing metastable GeSe by leveraging $AgInTe_2$ alloying and subsequent Pb doping to tailor the chemical bonding mechanisms. $AgInTe_2$ alloying fosters a transition from stable orthorhombic to metastable rhombohedral phase by substantially augmenting p–p electrons bonding to promote the formation of MVB. To prevent the transition of metastable rhombohedral to stable hexagonal phase at elevated temperatures, trace amounts of Pb are introduced to further strengthen the degree of MVB. This metastable rhombohedral phase showcases attributes of suitable bandgap, sharp valence band edge, elevated valley degeneracy, and convergence of multiple valence bands, which collectively contribute to decent carrier concentration, improved carrier mobility, and superior density-of-state effective mass compared to stable orthorhombic or hexagonal GeSe. Furthermore, the intrinsic characteristics of the metastable rhombohedral GeSe, such as the pronounced lattice anharmonicity, weak MVB, and multiscale lattice defects (point defects, domains, and nanoprecipitations), collaboratively suppress lattice thermal conductivity. Consequently, the $(Ge_{0.98}Pb_{0.02}Se)_{0.875}(AgInTe_2)_{0.125}$ achieves a peak zT of 1.0 at 773 K and an average zT of 0.53 between 298 and 773 K. A single-leg GeSe-based TE device was successfully engineered, exhibiting a maximum energy conversion efficiency of 4.90% and a power density of 1.12 W cm^{-2} under a 500 K temperature gradient. This work highlights the potential of enhancing the degree of MVB to stabilize metastable phases in GeSe and analogous p-bonded chalcogenides, thus paving a novel pathway for breakthroughs in the innovation of TE material.

AUTHOR CONTRIBUTIONS

Lipeng Hu supervised this project. Tu Lyu and Lipeng Hu conceived and designed this work, as well as wrote the manuscript. Yilun Huang conducted the investigation, experiment, and data analysis, and prepared the figures. Manting Zeng and Moran Wang contributed to the experiment. Yuan Yu reviewed and commented on this work and performed the validation. Min Hong performed the DFT calculations and data analysis and contributed to software. Tu Lyu, Min Hong, and Lipeng Hu discussed the results and revised and edited this manuscript. Chaohua Zhang and Fusheng Liu conducted the form analysis. All authors discussed the final manuscript.

ACKNOWLEDGMENTS

The work is financially supported by the National Key R&D Program of China (2021YFB1507403), the National Natural Science Foundation of China (52071218), the China Postdoctoral Science Foundation (2022M722170), and the Shenzhen University 2035 Program for Excellent Research (00000218). The authors appreciate Professor Qian Zhang, Professor Jun Mao, Li Yin, and Jinxuan Cheng from Harbin Institute of Technology (Shenzhen) for thermoelectric module fabrication and measurement. The authors thank the Instrumental Analysis Center of Shenzhen University.

CONFLICT OF INTEREST STATEMENT

The authors declare no conflict of interest.

ORCID

Lipeng Hu http://orcid.org/0000-0002-9682-8173

REFERENCES

[1] Xiao T, Nagaoka Y, Wang X, et al. Nanocrystals with metastable high-pressure phases under ambient conditions. *Science*. 2022;377(6608):870-874.

[2] Ostwald W. *Lehrbuch der allgemeinen chemie*. Wilhelm Engelman; 1893.

[3] Palumbo M, Battezzati L. Thermodynamics and kinetics of metallic amorphous phases in the framework of the CALPHAD approach. *Calphad*. 2008;32(2):295-314.

[4] Tan X, Geng S, Ji Y, et al. Closest packing polymorphism interfaced metastable transition metal for efficient hydrogen evolution. *Adv Mater*. 2020;32(40):2002857.

[5] Bundy FP. The P, T phase and reaction diagram for elemental carbon, 1979. *J Geophys Res Solid Earth*. 1980;85(B12):6930-6936.

[6] Zhao W, Pan J, Fang Y, et al. Metastable MoS_2: crystal structure, electronic band structure, synthetic approach and intriguing physical properties. *Chem Eur J*. 2018;24(60):15942-15954.

[7] He J, Tritt TM. Advances in thermoelectric materials research: looking back and moving forward. *Science*. 2017;357(6358):eaak9997.

[8] Zhu T, Liu Y, Fu C, Heremans JP, Snyder JG, Zhao X. Compromise and synergy in high-efficiency thermoelectric materials. *Adv Mater*. 2017;29(14):1605884.

[9] Li P, Qiu P, Xu Q, et al. Colossal nernst power factor in topological semimetal $NbSb_2$. *Nat Commun*. 2022;13(1):7612.

[10] Jiang B, Yu Y, Cui J, et al. High-entropy-stabilized chalcogenides with high thermoelectric performance. *Science*. 2021;371(6531):830-834.

[11] Fan Y, Xie C, Li J, et al. Engineering thermoelectric performance of α-GeTe by ferroelectric distortion. *Energy Environ Mater*. 2022;7(2):e12535.

[12] Liu Z, Hong T, Xu L, et al. Lattice expansion enables interstitial doping to achieve a high average zT in n-type PbS. *Interdiscip Mater*. 2023;2(1):161-170.

[13] He R, Schierning G, Nielsch K. Thermoelectric devices: a review of devices, architectures, and contact optimization. *Adv Mater Technol*. 2018;3(4):1700256.

[14] Yang D, Xing Y, Wang J, et al. Multifactor roadmap for designing low-power-consumed micro thermoelectric thermostats in a closed-loop integrated 5G optical module. *Interdiscip Mater*. 2024;3(2):326-337.

[15] Xie H, Zhao L-D, Kanatzidis MG. Lattice dynamics and thermoelectric properties of diamondoid materials. *Interdiscip Mater*. 2024;3(1):5-28.

[16] Zhang W, Lou Y, Dong H, et al. Phase-engineered high-entropy metastable fcc $Cu_{2-y}Ag_y(In_xSn_{1-x})Se_2S$ nanomaterials with high thermoelectric performance. *Chem Sci*. 2022;13(35):10461-10471.

[17] Pei J, Cai B, Zhuang H-L, Li J-F. Bi_2Te_3-based applied thermoelectric materials: research advances and new challenges. *Natl Sci Rev*. 2020;7(12):1856-1858.

[18] Shi H, Su L, Bai S, et al. Realizing high in-plane carrier mobility in n-type SnSe crystals through deformation potential modification. *Energy Environ Sci*. 2023;16(7):3128-3136.

[19] Zhu Y-K, Jin Y, Zhu J, et al. Design of n-type textured Bi_2Te_3 with robust mechanical properties for thermoelectric microrefrigeration application. *Adv Sci*. 2023;10(6):2206395.

[20] Tang X, Li Z, Liu W, Zhang Q, Uher C. A comprehensive review on Bi_2Te_3-based thin films: thermoelectrics and beyond. *Interdiscip Mater*. 2022;1(1):88-115.

[21] Wei T-R, Qiu P, Zhao K, Shi X, Chen L. Ag_2Q-based (Q = S, Se, Te) silver chalcogenide thermoelectric materials. *Adv Mater*. 2023;35(1):2110236.

[22] Tang Y, Yu Y, Zhao N, et al. High-performance thermoelectric α-$Ag_9Ga_{1-x}Te_6$ compounds with ultralow lattice thermal conductivity originating from Ag_9Te_2 motifs. *Angew Chem Int Ed*. 2022;61(36):e202208281.

[23] Hu L, Luo Y, Fang Y-W, et al. High thermoelectric performance through crystal symmetry enhancement in triply doped diamondoid compound Cu_2SnSe_3. *Adv Energy Mater*. 2021;11(42):2100661.

[24] Xu S, Zhou H, Sun Z, Xie J. Formation of an fcc phase through a bcc metastable state in crystallization of charged colloidal particles. *Phys Rev E*. 2010;82(1):010401.

[25] Lyu T, Li X, Yang Q, et al. Stepwise Ge vacancy manipulation enhances the thermoelectric performance of cubic GeSe. *Chem Eng J*. 2022;442:136332.

[26] Li X, Liang Z, Li J, et al. Crystal symmetry enables high thermoelectric performance of rhombohedral $GeSe(MnCdTe_2)_x$. *Nano Energy*. 2022;100:107434.

[27] Wang Z, Wu H, Zhang B, et al. Phase modulation enabled high thermoelectric performance in polycrystalline $GeSe_{0.75}Te_{0.25}$. *Adv Funct Mater*. 2022;32(26):2111238.

[28] Sarkar D, Roychowdhury S, Arora R, et al. Metavalent bonding in GeSe leads to high thermoelectric performance. *Angew Chem Int Ed*. 2021;60(18):10350-10358.

[29] Yan M, Geng H, Jiang P, Bao X. Glass-like electronic and thermal transport in crystalline cubic germanium selenide. *J Energy Chem*. 2020;45:83-90.

[30] Sist M, Gatti C, Nørby P, et al. High-temperature crystal structure and chemical bonding in thermoelectric germanium selenide (GeSe). *Chem Eur J*. 2017;23(28):6888-6895.

[31] Huang Z, Miller SA, Ge B, et al. High thermoelectric performance of new rhombohedral phase of GeSe stabilized through alloying with $AgSbSe_2$. *Angew Chem Int Ed*. 2017;56(45):14113-14118.

[32] Lencer D, Salinga M, Grabowski B, Hickel T, Neugebauer J, Wuttig M. A map for phase-change materials. *Nat Mater*. 2008;7(12):972-977.

[33] Yu Y, Zhou C, Ghosh T, et al. Doping by design: enhanced thermoelectric performance of GeSe alloys through metavalent bonding. *Adv Mater*. 2023;35(19):2300893.

[34] Hu L, Duan B, Lyu T, et al. In situ design of high-performance dual-phase GeSe thermoelectrics by tailoring chemical bonds. *Adv Funct Mater*. 2023;33(17):2214854.

[35] Lewis GN. The atom and the molecule. *J Am Chem Soc*. 1916;38(4):762-785.

[36] Wuttig M, Schön C-F, Lötfering J, Golub P, Gatti C, Raty JY. Revisiting the nature of chemical bonding in chalcogenides to explain and design their properties. *Adv Mater*. 2023;35(20):2208485.

[37] Yu Y, Cagnoni M, Cojocaru-Mirédin O, Wuttig M. Chalcogenide thermoelectrics empowered by an unconventional bonding mechanism. *Adv Funct Mater*. 2020;30(8):1904862.

[38] Guarneri L, Jakobs S, von Hoegen A, et al. Metavalent bonding in crystalline solids: how does it collapse? *Adv Mater*. 2021;33(39):2102356.

[39] Duan B, Zhang Y, Yang Q, et al. The role of cation vacancies in GeSe: stabilizing high-symmetric phase structure and enhancing thermoelectric performance. *Adv Energy Sustain Res*. 2022;3(11):2200124.

[40] Xu X, Xie L, Lou Q, Wu D, He J. Boosting the thermoelectric performance of pseudo-layered $Sb_2Te_3(GeTe)_n$ via vacancy engineering. *Adv Sci*. 2018;5(12):1801514.

[41] Zhong J, Liang G, Cheng J, et al. Entropy engineering enhances the thermoelectric performance and microhardness of $(GeTe)_{1-x}(AgSb_{0.5}Bi_{0.5}Te_2)_x$. *Sci China Mater*. 2023;66(2):696-706.

[42] Xu M, Jakobs S, Mazzarello R, et al. Impact of pressure on the resonant bonding in chalcogenides. *J Phys Chem C*. 2017;121(45):25447-25454.

[43] Raty J-Y, Wuttig M. The interplay between peierls distortions and metavalent bonding in IV–VI compounds: comparing GeTe with related monochalcogenides. *J Phys D Appl Phys*. 2020;53(23):234002.

[44] Wang Z, Wu H, Xi M, et al. Structure-dependent thermoelectric properties of $GeSe_{1-x}Te_x$ ($0 \le x \le 0.5$). *ACS Appl Mater Interfaces*. 2020;12(37):41381-41389.

[45] Littlewood PB. The crystal structure of IV-VI compounds. I. Classification and description. *J Phys C Solid State Phys*. 1980;13(26):4855-4873.

[46] Arora R, Waghmare UV, Rao CNR. Metavalent bonding origins of unusual properties of group IV chalcogenides. *Adv Mater*. 2023;35(7):2208724.

[47] Cagnoni M, Führen D, Wuttig M. Thermoelectric performance of IV–VI compounds with octahedral-like coordination: a chemical-bonding perspective. *Adv Mater*. 2018;30(33):1801787.

[48] Küpers M, Konze PM, Maintz S, et al. Unexpected Ge–Ge contacts in the two-dimensional Ge_4Se_3Te phase and analysis of their chemical cause with the density of energy (DOE) function. *Angew Chem Int Ed*. 2017;56(34):10204-10208.

[49] Yao Z, Li W, Tang J, et al. Solute manipulation enabled band and defect engineering for thermoelectric enhancements of SnTe. *InfoMat*. 2019;1(4):571-581.

[50] Zhang X, Shen J, Lin S, et al. Thermoelectric properties of GeSe. *J Materiomics*. 2016;2(4):331-337.

[51] Hong M, Wang Y, Feng T, et al. Strong phonon–phonon interactions securing extraordinary thermoelectric $Ge_{1-x}Sb_xTe$ with Zn-alloying-induced band alignment. *J Am Chem Soc*. 2019;141(4):1742-1748.

[52] Su D, Cheng J, Li S, et al. Inhibiting the bipolar effect via band gap engineering to improve the thermoelectric performance in n-type $Bi_{2-x}Sb_xTe_3$ for solid-state refrigeration. *J Mater Sci Technol*. 2023;138:50-58.

[53] Hu L, Meng F, Zhou Y, et al. Leveraging deep levels in narrow bandgap $Bi_{0.5}Sb_{1.5}Te_3$ for record-high zT_{ave} near room temperature. *Adv Funct Mater*. 2020;30(45):2005202.

[54] Moshwan R, Yang L, Zou J, Chen Z-G. Eco-friendly SnTe thermoelectric materials: progress and future challenges. *Adv Funct Mater*. 2017;27(43):1703278.

[55] May AF, Toberer ES, Saramat A, Snyder GJ. Characterization and analysis of thermoelectric transport in *n*-type $Ba_8Ga_{16-x}Ge_{30+x}$. *Phys Rev B Condens Matter Mater Phys*. 2009;80(12):125205.

[56] Yan M, Tan X, Huang Z, Liu G, Jiang P, Bao X. Synergetic optimization of electronic and thermal transport for high-performance thermoelectric $GeSe–AgSbTe_2$ alloy. *J Mater Chem A*. 2018;6(18):8215-8220.

[57] Yao W, Zhang Y, Lyu T, et al. Two-step phase manipulation by tailoring chemical bonds results in high-performance GeSe thermoelectrics. *Innovation*. 2023;4(6):100522.

[58] Lee S, Esfarjani K, Luo T, Zhou J, Tian Z, Chen G. Resonant bonding leads to low lattice thermal conductivity. *Nat Commun*. 2014;5(1):3525.

[59] Zhu J, Xie L, Ti Z, et al. Computational understanding and prediction of 8-electron half-heusler compounds with unusual suppressed phonon conduction. *Appl Phys Rev*. 2023;10(3):031405.

[60] Han S, Dai S, Ma J, et al. Strong phonon softening and avoided crossing in aliovalence-doped heavy-band thermoelectrics. *Nat Phys*. 2023;19(11):1649-1657.

[61] Chen Z, Zhang X, Lin S, Chen L, Pei Y. Rationalizing phonon dispersion for lattice thermal conductivity of solids. *Natl Sci Rev*. 2018;5(6):888-894.

[62] Wang X, Yao H, Yin L, et al. Band modulation and strain fluctuation for realizing high average *zT* in GeTe. *Adv Energy Mater*. 2022;12(26):2201043.

SUPPORTING INFORMATION

Additional supporting information can be found online in the Supporting Information section at the end of this article.

How to cite this article: Huang Y, Lyu T, Zeng M, et al. Manipulation of metavalent bonding to stabilize metastable phase: a strategy for enhancing *zT* in GeSe. *Interdiscip Mater*. 2024;3:607-620. doi:10.1002/idm2.12170